Atom-interferometric gravitational-wave detection using heterodyne laser links

Jason M. Hogan and Mark A. Kasevich
Department of Physics, Stanford University, Stanford, California 94305, USA
(Received 22 March 2015; revised manuscript received 17 August 2016; published 28 September 2016)

We propose a gravitational-wave detection method based on heterodyne laser links and light-pulse atom interferometry that enables high sensitivity gravitational-wave detection in the 0.1-mHz to 1-Hz frequency band using a single, long ($>10^8$ m), detector baseline. The detection baseline in previous atom-based proposals was constrained by the need for a reference laser to remain collimated over the optical propagation path between two satellites. Here we circumvent this requirement by employing a strong local oscillator laser near each atom ensemble that is phase referenced or phase locked to the reference laser beam. Longer baselines offer a number of potential advantages, including enhanced sensitivity, simplified atom optics, and reduced atomic source flux requirements.

DOI: 10.1103/PhysRevA.94.033632

I. INTRODUCTION

Atom interferometry offers a potential strategy for high-sensitivity gravitational-wave detection in the 0.1-mHz to 1-Hz frequency band. Strengths of the atom-interferometric approach include phase multiplication through multiple pulse sequences, proof mass resilience [1], laser frequency noise immunity, and quantum back-action noise immunity [2].

In previous proposals, technical considerations have limited the possible baseline length of the detector. In this article, we describe a method which enables antenna operation with substantially longer baselines. This results in designs whose sensitivities exceed those of existing proposals (e.g., LISA [3]), but which do not require significant advances in the state of the art for atom interferometry. For example, we describe an antenna with ten times the sensitivity of the LISA antenna that invokes 12 photon recoil atom optics.

In a single-baseline atom-interferometric detector, the light pulses are sent back and forth across the baseline from alternating directions, driving single-photon transitions in the atoms on both ends [2]. Momentum recoil from the interactions generates the interferometers, whose phases reflect the relative motion of the atoms with respect to the optical phase fronts. The phase difference between the two interferometers is sensitive to variations of the light travel time across the baseline, so by monitoring the phase difference it is possible to detect travel time fluctuations induced by gravitational waves (GWs). Previous proposals have assumed that the atom optics laser beam is collimated, constraining the allowed baseline length L to no larger than the Rayleigh range z_R of the laser: $L \leqslant 2z_R = 2\pi w^2/\lambda$, where λ is the laser wavelength and w is the radial beam waist [2,4]. Assuming $(\Omega/2\pi) \sim$ kHz Rabi frequencies with 1-m telescopes and 10-W laser power sets a practical limit for a baseline length of $L \sim 10^3$ km [2,4].

Although atom-interferometric detectors operating at 1000 km have the potential to reach comparable sensitivity to LISA [4], the advantages of increasing the baseline are tantalizing. Generally, a local acceleration noise source δa results in an effective strain response $\propto \delta a/L$, so longer baselines reduce the technical requirements needed to control a wide class of backgrounds. Furthermore, at the same target GW signal strength, increasing the baseline reduces the need to use large momentum transfer (LMT) and other phase enhancement techniques [2,5], simplifying the interferometer operation. Finally, enhanced strain sensitivity allows for increased science reach.

II. HETERODYNE LASER LINK

A. Setup

In our proposal, intense local lasers are used to operate the atom interferometers at each end of the baseline. To connect these otherwise independent local lasers, reference laser beams are transmitted between the two spacecraft, and the local lasers are phase referenced or phase locked to the incoming wave fronts of these reference lasers. In this scheme, the reference beams do not need to be collimated, since the phase locks can be done using much less intensity than is required to drive the atomic transitions. This allows the baseline to be extended to LISA-like lengths with only a modest telescope size and reference beam power. Critically, since the phase-locked (or phase-referenced) local laser tracks the noise of the incoming reference laser, this arrangement maintains the essential common-mode laser phase noise cancellation between the two interferometers that allows for single baseline operation. This noise immunity is a fundamental difference from other proposals that use heterodyne links for extended baselines [3,6]. The current proposal effectively decouples the phase noise rejection requirement from the atom optics intensity demands, allowing the flexibility to independently optimize the baseline and atomic transition rate.

A schematic is shown in Fig. 1. Each satellite contains an atom interferometer that is implemented using alternating laser pulses traveling along the positive and negative z directions. Both satellites contain their own master laser (M1 and M2) that has enough intensity to drive transitions in the local atom interferometer. After interacting with the local atom cloud, the master laser beam exits the satellite through a beamsplitter and then propagates across the baseline towards the opposite satellite. We refer to the beams propagating between the satellites as reference beams: R1 and R2 are the reference beams originating from satellite 1 and 2, respectively.

The reference beams are not assumed to be collimated when they reach the opposite satellite, so for very long baselines the

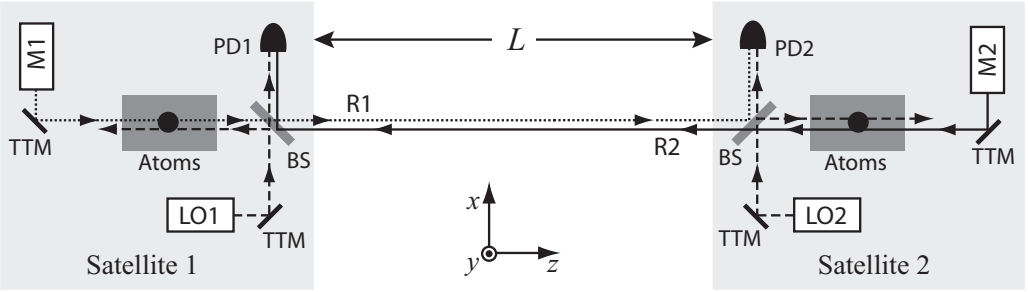

FIG. 1. Schematic of the proposed design. M1 and M2 are the master lasers, with beams depicted as dotted and solid lines, respectively. The reference beams propagating between the satellites are denoted R1 (dotted) and R2 (solid). LO1 and LO2 are local oscillator lasers (dashed beam lines) that are phase locked to the incoming reference laser beams (R2 and R1, respectively). PD1 (PD2) is a photodetector used to measure the heterodyne beat note between the incoming reference beam R2 (R1) and the local oscillator laser LO1 (LO2) in order to provide feedback for the laser link. BS is a (nonpolarizing) beamsplitter where the heterodyne beat note is formed. Tip-tilt mirrors (TTMs) allow for fine control of the pointing direction of each laser. All adjacent parallel beams are nominally overlapped, but for clarity they are shown here with a small offset.

received reference beam intensity is expected to be too low to directly drive an atomic transition. To address this, local oscillator lasers (LO1 and LO2) are phase referenced to the incoming reference beams, and these lasers have sufficient intensity to drive transitions in the local atom interferometers. The phase reference for laser LO1 is implemented by detecting the heterodyne beat note formed by the incoming reference beam R2 with laser LO1 on the beamsplitter BS in satellite 1 (and analogously for LO2 in satellite 2). In addition to a photodetector for measuring the phase difference between the two beams, a quadrant detector (or camera) may be used to characterize the spatial interference pattern. This allows the pointing direction and spatial mode of the two lasers to be well matched using appropriate feedback, as discussed later. Finally, note that the two lasers on a given satellite (e.g., M1 and LO1) do not have to be tightly locked together, because noise from each laser direction independently cancels in the phase difference between the two interferometers [7].

B. Laser phase noise

An essential consideration is the required noise performance of the phase reference measurement between the reference beam and the local oscillator in each satellite. Any noise added by the phase reference is not common between the interferometers and so must be sufficiently small.

Consider the laser phase noise arising from one of the pulses in the interferometer sequence. For concreteness, we analyze a pulse propagating in the positive z direction from satellite 1 to satellite 2. During the pulse, the phase of the master laser M1 generally evolves in time as $\phi_M(t)$. When this pulse later arrives at satellite 2 after propagating across the baseline, the received reference beam R1 will also vary as $\phi_M(t)$, while the local oscillator laser LO2 evolves as $\phi_{LO}(t)$. For a pulse of duration τ beginning at time t_0, the atom records a weighted average of the laser phase evolution $\langle\phi(t)\rangle \equiv \frac{1}{\tau}\int_{t_0}^{t_0+\tau} w(t)\phi(t)\,dt$, where $w(t) \equiv \frac{\Omega(t)\tau}{2}\sin\left(\int_{t_0}^{t}\Omega(t')dt'\right)$ is a dimensionless weighting function [8], and $\Omega(t)$ is the time-dependent Rabi frequency that defines the pulse envelope [9,10]. Thus $\langle\phi_M(t)\rangle$ and $\langle\phi_{LO}(t)\rangle$ are imprinted on the atoms in satellite 1 and 2, respectively, and the phase difference between the atom interferometers has a laser noise contribution $\delta\phi_L = \langle\phi_M(t)\rangle - \langle\phi_{LO}(t)\rangle$.

This noise can be suppressed by incorporating the optical phase reference measurement, which in this example is the heterodyne signal present on PD2. The heterodyne beat note on PD2 evolves as $\Delta\Phi_{\rm PD}(t) = \phi_M(t) - \phi_{LO}(t)$ during the pulse. In one possible implementation, this measurement can be used to lock the phase of LO2 in real time to the reference beam [11], ensuring $\phi_M(t) = \phi_{LO}(t)$. In the case of a phase lock we then have $\langle\phi_M(t)\rangle = \langle\phi_{LO}(t)\rangle$, so the laser noise contribution $\delta\phi_L$ to the interferometer phase difference vanishes. Alternatively, LO2 can be left to evolve freely, and the heterodyne signal can be used as a phase reference that is later combined with the atom signals to remove the noise $\delta\phi_L$. In this case, the heterodyne data may need to be time averaged with the appropriate weighting function $w(t)$ to accurately match the atom response. This corresponds to matching the optical heterodyne and atomic phase transfer functions in the frequency domain.

C. Vibration noise

Another source of phase noise could arise from motion of the beamsplitter (BS). The beamsplitter is assumed to be rigidly connected to the satellite bus, so any platform vibration noise will affect the beamsplitter as well. However, it turns out that the proposed scheme is insensitive to phase noise introduced by vibration of the beamsplitters.

To see this, assume that the heterodyne reference is operated in a phase locked mode, and that the incoming reference laser has phase $\phi_{\rm R}$ at the nominal position $\mathbf{r} = 0$ of the beamsplitter. Due to vibration of the satellite, the beamsplitter may be displaced by some amount $\mathbf{\Delta r}$, so upon reflection from the beamsplitter the reference beam will instead have phase $\phi'_{\rm R} = \phi_{\rm R} + \mathbf{k}\cdot\mathbf{\Delta r}$, where $\mathbf{k}$ is the wave vector of the incoming reference beam. On the other hand, the LO beam that transmits through the beamsplitter is not impacted by the displacement, so the heterodyne signal between the lasers encodes the vibration noise $\mathbf{\Delta r}$. When the phase lock is engaged, the phase of the LO laser $\phi_{\rm LO}$ at $\mathbf{r} = 0$ is locked to the phase of the reflected reference beam, resulting in $\phi_{\rm LO} = \phi_{\rm R} + \mathbf{k}\cdot\mathbf{\Delta r}$. Finally, consider the phase $\phi'_{\rm LO}$ of the LO beam that reflects

off the beamsplitter and that is subsequently incident on the atoms. Since the LO beam reflects off the opposite side of the beamsplitter compared to the reference beam, the reflected LO beam at $\mathbf{r} = 0$ has phase $\phi'_{\rm LO} = \phi_{\rm LO} - \mathbf{k}\cdot\boldsymbol{\Delta}\mathbf{r}$. This implies that $\phi'_{\rm LO} = \phi_{\rm R}$ as desired, so the vibration noise does not affect the light reaching the atoms. A similar argument holds when the heterodyne signal is used as a phase reference rather than a phase lock, since any phase shift added to the LO upon reflection off the beamsplitter will also be present on the heterodyne signal, and so can later be subtracted.

D. Photon shot noise

The phase reference is ultimately limited by photon shot noise of the received reference beam light. This is a constraint that has not been present in past designs based on collimated beams. Since both atom interferometers are driven using high intensity local lasers, photon shot noise does not directly contribute to phase noise of the atom-interferometer signals. Rather, photon shot noise limits the ability to measure the heterodyne beat note $\Delta\Phi_{\rm PD}(t)$ during the finite duration of each interferometer pulse. To avoid limiting the strain resolution, the photon shot noise contribution to the detector noise budget must be less than the contribution from atom shot noise.

For the time-average heterodyne phase measurement $\langle\Delta\Phi_{\rm PD}(t)\rangle$, the variance is given by the number of photons N_γ received during a pulse: $\mathrm{Var}[\langle\Delta\Phi_{\rm PD}(t)\rangle] = 1/N_\gamma$. This may be written as a product of the pulse bandwidth and the phase noise power spectral density (PSD) of the shot noise $S_{\rm sh} = h\nu/P_r$, where P_r is the power of the received reference beam and $\nu = c/\lambda$ is the light frequency. For an interferometer consisting of n_p (uncorrelated) pulses, the rms phase uncertainty contributed by the heterodyne reference is then $\delta\phi^2_{\rm rms} = \mathrm{Var}[\langle\Delta\Phi_{\rm PD}(t)\rangle] = n_p S_{\rm sh}\Omega$, where we take the Rabi frequency Ω as the effective bandwidth of a single pulse. Assuming an atom-interferometer repetition rate of f_R, the associated noise PSD is $\overline{\delta\phi}^2_\gamma = \delta\phi^2_{\rm rms}/f_R$.

For a Gaussian beam with power P_t and radial waist w_t at the transmitting satellite, the received power collected by a telescope with diameter d is $P_r \approx \frac{1}{2}P_t(d/w_r)^2$ for $d \ll w_r$, where $w_r \approx L\lambda/\pi w_t$ is the reference beam waist after propagating a distance $L \gg z_{\rm R}$ to the receiving satellite location. The Rabi frequency $\Omega = \Gamma\sqrt{I_t/2I_{\rm sat}}$ is set by the intensity $I_t = \frac{P_t}{\pi w_t^2/2}$ at the transmitting satellite. The final noise amplitude spectral density is then

$$\overline{\delta\phi}_\gamma = \sqrt[4]{\frac{1536\,\hbar c}{\pi^5}}\,\frac{n_p^{1/2}\Gamma^{1/4}\lambda^{5/4}L}{f_R^{1/2}P_t^{1/4}d^{5/2}}, \tag{1}$$

where the telescope diameter is taken to be $d = 2w_t$. In this expression, we assume a two-level transition with saturation intensity $I_{\rm sat} = 2\pi^2\hbar c\,\Gamma/3\lambda^3$ (Γ is the transition natural linewidth). By comparison, the phase noise PSD of atom shot noise is $\overline{\delta\phi}^2_a = 1/\dot{N}_a$, where $\dot{N}_a$ is the mean number of detected atoms per unit time that participate in the atom-interferometer signal. In designing the laser link phase reference we require that $\overline{\delta\phi}_\gamma \leqslant \overline{\delta\phi}_a$. Assuming the Sr clock transition, the telescope diameter is constrained to be

$$d = 28\ \mathrm{cm}\left(\frac{L}{2\times10^9\ \mathrm{m}}\right)^{2/5}\left(\frac{1\mathrm{W}}{P_t}\right)^{1/10}\left(\frac{0.2\mathrm{Hz}/7}{f_R/n_p}\right)^{1/5} \times\left(\frac{\overline{\delta\phi}_a}{10^{-3}/\sqrt{\mathrm{Hz}}}\right)^{2/5}, \tag{2}$$

where $n_p = 7$ corresponds to a $2\hbar k$ interferometer [2].

III. GRAVITATIONAL-WAVE PHASE SHIFT

Here we outline the calculation of the phase shift in the atom interferometer in response to a passing gravitational wave. We assume the usual gradiometer configuration [4] for gravitational-wave detection and compute the differential phase shift between two atom interferometers separated by a baseline of length L. The interferometers are assumed to use single-photon transitions, and large momentum transfer (LMT) atom optics are implemented by driving transitions from alternating directions [2]. In order to model interleaved interferometer operation, we use realistic pulse sequences that allow for multiple concurrent atom interferometers. The pulse timings for a single interferometer are therefore chosen with appropriate gaps so that these other concurrent interferometers can be simultaneously addressed with minimal crosstalk.

The basic calculation method is described in previous work [2,4]. Here we apply those methods to an interleaved LMT single-photon interferometer sequence. The interferometer phase shift nominally consists of three parts: the propagation phase, laser phase, and separation phase. However, for the interferometers considered here, the only important contribution to the gravitational-wave signal comes from propagation phase.

In a gradiometer between two single-photon interferometers sharing the same laser pulses, the laser phase associated with every pulse is common to both interferometers, and cancels on a pulse-by-pulse basis in the phase difference between them [2]. Thus for calculating the GW signal we can ignore laser phase. Separation phase can arise in a single-photon interferometer in response to a gravitational wave, but it is usually much smaller than the primary GW signal and can be neglected. To see this, note that the separation phase can be attributed to a differential acceleration between the two paths of the interferometer that leads to an offset between the wave packets at the end of the sequence. The differential acceleration between the paths from a GW of strain h and frequency ω is roughly $\sim h\Delta x\omega^2$, where Δx is the separation between the interferometer paths (the wave-packet separation). By comparison, the typical GW differential acceleration signal between the two interferometers in the gradiometer of baseline L is $\sim hL\omega^2$ [2]. Since $L \gg \Delta x$ in the configurations we consider here, we can typically neglect any signal that could arise from separation phase. This approximation can be verified by explicit calculation of the separation phase, but here we omit this for simplicity.

The relevant GW signal in the gradiometer therefore originates from the propagation phase. The signal may be qualitatively understood in the following way. As the atom's internal state is modulated by the sequence of laser pulses, the two paths of the atom interferometer spend slightly different

amounts of time in the excited state due to the GW. Indeed, the nominal symmetry between the two paths in a three pulse accelerometer sequence ($\pi/2 - \pi - \pi/2$ and its LMT generalizations) is broken by the gravitational wave. The GW modulates the time it takes light to cross the baseline between the two interferometers. This changes the arrival time of the light pulses, which in turn affects the amount of time that the atoms spend in the excited state, leading to a phase shift [2].

For the phase shift calculation we use the following metric written in the TT gauge for a plane gravitational-wave traveling the z direction:

$$\begin{aligned} ds^2 =& c^2dt^2 - dx^2 - dy^2 - dz^2 \\ &+ h_+(t)(dx^2 - dy^2) - 2h_\times(t)dxdy, \end{aligned} \tag{3}$$

where $h_+(t) = h_+ \cos[\omega(t - \frac{z}{c}) + \phi_0]$ and $h_\times(t) = h_\times \cos[\omega(t - \frac{z}{c}) + \phi_0]$ are the strain amplitudes for plus and cross polarization, respectively, ω is the GW frequency, and ϕ_0 is an arbitrary reference phase. To model the response to GW sources arriving with arbitrary direction, we keep the metric fixed and orient the baseline of the interferometer along the unit three-vector $\mathbf{n} = (\sin\theta\cos\phi, \sin\theta\sin\phi, \cos\theta)$.

Calculating the propagation phase shift amounts to first determining the geometry of the interferometer by finding the intersection points of the light geodesics with the atom geodesics. These intersection points define the boundaries of a series of interferometer path segments. For each path segment, we calculate the proper time interval along the segment using the metric and then multiply by the appropriate internal energy (rest mass) associated with that path segment.

As an additional simplification, we can typically neglect photon recoil effects on the atom trajectories and simply assume the two atom paths of the interferometer are at a fixed coordinate position. Note that in the chosen coordinate system, a fixed coordinate position is a valid solution to the geodesic equation for an atom. In reality, due to the exchange of momentum with the light at each pulse, the two paths of the interferometer do not stay on this initial geodesic and there is a finite wave-packet separation. However, ignoring this effect once again amounts to neglecting a very small correction to the GW signal that is proportional to the wave-packet separation Δx.

Therefore, neglecting recoil effects, the geodesics for the two atom-interferometer paths are both adequately approximated by $x^\mu_{\text{atom}} = (t, \mathbf{n}\, r)$, where $r = \sqrt{x^2 + y^2 + z^2}$ is the constant coordinate distance of the atom from the origin. The propagation phase along the ith segment of the interferometer then reduces to

$$\delta\phi_i = \frac{c}{\hbar}\int m_i ds = \frac{m_i c^2}{\hbar}\Delta t_i \tag{4}$$

where Δt_i is the coordinate time difference between the start and end of the segment and m_i is the atom mass along the segment (including internal energy). This result follows from the fact that along the atom geodesic x^μ_{atom} we have $dx = dy = dz = 0$, and so from the metric $ds = cdt$. The total propagation phase shift is then

$$\Delta\Phi_{\text{prop}} = \sum_{\{u_i\}}\delta\phi_i - \sum_{\{l_i\}}\delta\phi_i, \tag{5}$$

where the sums are over the set of all upper segments $\{u_i\}$ and lower segments $\{l_i\}$ of the interferometer.

Without loss of generality, we take the baseline of the detector to run through the origin along the direction given by $\mathbf{n}$. The laser pulses are assumed to originate at radial position r_{in} and r_{out} along this same line, with $r_{\text{in}} < r < r_{\text{out}}$. Light pulses that depart from the laser at r_{in} must propagate in the $(+\mathbf{n})$ direction to reach the atom at r, while pulses from r_{out} must propagate in the $(-\mathbf{n})$ direction. The pulses leave from each laser at scheduled proper time intervals as measured by each laser locally. However since both lasers are also on geodesics with $dx = dy = dz = 0$, the proper time of the lasers is equal to the coordinate time t.

To determine the geometry of the interferometer segments and their time durations Δt_i, we must calculate the arrival times at the atom position of the null geodesics of the light pulses. Solutions to the geodesic equations derived from metric Eq. (3) are well known [12] and will not be reproduced here in the interest of brevity. For a null geodesic leaving the laser at coordinate time t_0, the arrival time at the atom is found to be

$$\begin{aligned} t_\pm =& t_0 + \frac{|r - r_0|}{c} + \frac{1 \mp \cos\theta}{2\omega}(h_+\cos 2\phi + h_\times \sin 2\phi) \\ &\times \left[\sin\left(\frac{\omega|r - r_0|}{c} + \frac{\omega r}{c}\cos\theta + \omega t_0 + \phi_0\right)\right. \\ &\left. - \sin\left(\frac{\omega r_0}{c}\cos\theta + \omega t_0 + \phi_0\right)\right], \end{aligned} \tag{6}$$

where r_0 is the initial radial position of the null geodesic (either r_{in} or r_{out}) and r is once again the position of the atom. Here t_+ is the arrival time for a light pulse propagating in the $(+\mathbf{n})$ direction from r_{in} and t_- is for a pulse propagating in the $(-\mathbf{n})$ direction from r_{out}.

The pulse sequence for a $2\hbar k$ interferometer using single photon transitions is shown in Table I. The pulse timing for this sequence accounts for the light propagation delay L/c across the baseline and assumes a duration τ for each pulse. Given these initial pulse times t_0 we can determine the arrival time of each of the pulses using Eq. (6) and then subsequently determine the propagation phase by substituting the resulting Δt_i into Eq. (5). We are ultimately interested in the differential phase between two atom interferometers, which we call the gradiometer phase response. Taking one interferometer to be located at $r = r_{\text{in}}$ and the other at $r = r_{\text{out}}$, the final $2\hbar k$ gradiometer phase response is

$$\begin{aligned} \Delta\Phi^{\text{grad}}_{2\hbar k}(\theta,\phi) =& \frac{8\omega_a}{\omega}\sin\left(\frac{\omega T}{2}\right)\left[\cos^2\frac{\theta}{2}\sin\left(\frac{\omega L}{c}\sin^2\frac{\theta}{2}\right)\right. \\ &\times \sin\left[\omega\left(\frac{T}{2} - \frac{L}{c} - \tau\right)\right] \\ &\left. + \sin^2\frac{\theta}{2}\sin\left(\frac{\omega L}{c}\cos^2\frac{\theta}{2}\right)\sin\left(\frac{\omega T}{2}\right)\right] \\ &\times (h_+\cos 2\phi + h_\times \sin 2\phi)\cos\widetilde{\phi}_0, \end{aligned} \tag{7}$$

where $\widetilde{\phi}_0 \equiv (\phi_0 + \omega T + \frac{\omega L}{c}\cos^2\frac{\theta}{2} + \frac{\omega r_{\text{in}}}{c}\cos\theta)$ encodes the phase of the GW at the start of the interferometer and we take $r_{\text{out}} = r_{\text{in}} + L$. This result represents the general $2\hbar k$ interferometer phase response to GWs with arbitrary angle of incidence and polarization.

TABLE I. Pulse sequence for a $2\hbar k$ interferometer using single-photon transitions. The initial coordinate time and position of the null geodesic associated with each pulse is given by t_0 and r_0, respectively. The direction of the pulse propagation is indicated by an arrow, where $\leftarrow$ means propagation in the $-\mathbf{n}$ direction and $\rightarrow$ means propagation in the $+\mathbf{n}$ direction. The detuning of each pulse with respect to the transition resonance is given in units of the recoil frequency ω_r and assumes the atom is initially at rest and that there is zero relative velocity between the lasers. The right two columns show the state of the atom along each path of the interferometer and indicate the transitions that are caused by each pulse. In addition to the momentum of the atom, the internal state is labeled by "g" for the ground state and "e" for the excited state.

Pulse	Area	Time t_0	r_0	Direction	Detuning (ω_r)	Upper Path	Lower Path
1	$\pi/2$	0	r_{in}	$\rightarrow$	1	$\lvert g,0\rangle \rightarrow \lvert e,\hbar k\rangle$	$\lvert g,0\rangle$
2	π	$\frac{L}{c}+\tau$	r_{out}	$\leftarrow$	-3	$\lvert e,\hbar k\rangle \rightarrow \lvert g,2\hbar k\rangle$	$\lvert g,0\rangle$
3	π	$T-\frac{L}{c}-\tau$	r_{out}	$\leftarrow$	-3	$\lvert g,2\hbar k\rangle \rightarrow \lvert e,\hbar k\rangle$	$\lvert g,0\rangle$
4	π	T	r_{in}	$\rightarrow$	1	$\lvert e,\hbar k\rangle \rightarrow \lvert g,0\rangle$	$\lvert g,0\rangle \rightarrow \lvert e,\hbar k\rangle$
5	π	$T+\frac{L}{c}+\tau$	r_{out}	$\leftarrow$	-3	$\lvert g,0\rangle$	$\lvert e,\hbar k\rangle \rightarrow \lvert g,2\hbar k\rangle$
6	π	$2T-\frac{L}{c}-\tau$	r_{out}	$\leftarrow$	-3	$\lvert g,0\rangle$	$\lvert g,2\hbar k\rangle \rightarrow \lvert e,\hbar k\rangle$
7	$\pi/2$	$2T$	r_{in}	$\rightarrow$	1	$\lvert g,0\rangle \rightarrow \lvert e,\hbar k\rangle$	$\lvert e,\hbar k\rangle \rightarrow \lvert g,0\rangle$

To compute the instrument sensitivity function, we calculate the average response of the detector over all angles and polarizations. Since we are interested in the magnitude of the signal, we may drop the $\cos\widetilde{\phi}_0$ oscillatory term (or equivalently, we sum the signal quadratures in the frequency domain to get the magnitude of the response). The rms response averaged over angle and polarization is

$$\Delta\Phi_{2\hbar k}^{\text{rms}} = \sqrt{\frac{1}{2}\sum_{+,\times}\left(\frac{1}{4\pi}\int_0^{2\pi}\int_0^{\pi}\left|\Delta\Phi_{2\hbar k}^{\text{grad}}(\theta,\phi)\right|^2\sin\theta\,d\theta d\phi\right)}, \tag{8}$$

where the sum indicates the average over both possible polarizations. Performing the integrals yields

$$\begin{aligned}\Delta\Phi_{2\hbar k}^{\text{rms}} =& \sqrt{8}h_{\text{rms}}\frac{\omega_a}{\omega}\sin^2\left(\frac{\omega T}{2}\right)\left\{\left(\frac{c^3}{2\omega^3L^3}\sin\left(\frac{2\omega L}{c}\right)\right.\right.\\ &-\frac{c^2}{L^2\omega^2}+\frac{2}{3}\left)\left[1+\frac{\sin^2\left[\omega\left(\frac{T}{2}-\frac{L}{c}-\tau\right)\right]}{\sin^2\left(\frac{\omega T}{2}\right)}\right]\right.\\ &+2\left[\frac{c^3}{\omega^3L^3}\sin\left(\frac{\omega L}{c}\right)-\left(\frac{c^2}{\omega^2L^2}+\frac{1}{3}\right)\cos\left(\frac{\omega L}{c}\right)\right]\\ &\left.\left.\times\frac{\sin\left[\omega\left(\frac{T}{2}-\frac{L}{c}-\tau\right)\right]}{\sin\left(\frac{\omega T}{2}\right)}\right\}^{1/2},\end{aligned} \tag{9}$$

where $h_{\text{rms}}=\sqrt{(h_+^2+h_\times^2)/2}$ is the rms GW strain.

The phase response given by Eq. (9) shows that the detector is insensitive at frequencies spaced by integer multiples of $2\pi/T$. This results in well-known nodes in the response curve at these frequencies, which can be undesirable. To mitigate this effect, it is possible to periodically change the value of T used by the interferometer. This moves the node frequencies around and ensures that, on average, the detector is not blind to any frequencies in the detection band. To model this procedure, we compute the rms of the phase response using several different T values:

$$\Delta\Phi_{2\hbar k}^{\text{rms},T} = \sqrt{\frac{1}{n}\sum_{i=1}^{n}\left|\Delta\Phi_{2\hbar k}^{\text{rms}}(T_i)\right|^2}. \tag{10}$$

This average over multiple sensitivity functions with different T is a valid description of the detector response on time scales longer than the cycle time through the set of T_i. In practice it is sufficient to use $n\sim 4$ to effectively smooth out the sensitivity curve, so the T_i cycle time is likely a small multiple of the detector sampling interval. Note that the particular choice of the T_i is important for optimizing the detector response. For instance, none of the T_i should be related by an integer multiple to any other in order to avoid having nodes in common.

To generate the sensitivity curve from the phase response, we find the minimum rms strain h_{rms} that can be resolved in the presence of a certain level of rms phase noise $\delta\phi_{\text{rms}}$. This amounts to solving $\Delta\Phi_{n\hbar k}^{\text{rms},T}=\delta\phi_{\text{rms}}$ for h_{rms} using either Eqs. (9) or (11) for $2\hbar k$ or $12\hbar k$, respectively. The sensitivity curve can also be expressed as a strain amplitude spectral density by replacing $\delta\phi_{\text{rms}}$ with the phase noise amplitude spectral density $\sqrt{S_\phi}$.

Following the same procedure, we also calculate the detector response for a $12\hbar k$ interferometer using the pulse sequence given in Table II. This pulse sequence allows for LMT multiplexing, so multiple simultaneous interferometers can be operated concurrently with minimal crosstalk between velocity channels. Given the complexity of the intermediate expressions, here we simply give the final result of the phase response after performing the average over polarization and direction:

$$\begin{aligned}\Delta\Phi_{12\hbar k}^{\text{rms}} =& \sqrt{8}h_{\text{rms}}\frac{\omega_a}{\omega}\sin^2\left(\frac{\omega L}{c}\right)\left\{\left[\text{sinc}\left(\frac{L\omega}{c}\right)-\cos\left(\frac{L\omega}{c}\right)\right]\left[\sum_{i=1}^{26}\Lambda_{2i-1}\cos\left(\frac{(2i-1)L\omega}{c}\right)\right]\right.\\ &\left.+\left[\text{sinc}\left(\frac{2L\omega}{c}\right)+\text{Cin}\left(\frac{2L\omega}{c}\right)-1\right]\left[\frac{\Lambda_0}{2}+\sum_{i=1}^{26}\Lambda_{2i}\cos\left(\frac{2iL\omega}{c}\right)\right]\right\}^{1/2}.\end{aligned} \tag{11}$$

TABLE II. Pulse sequence for a $12\hbar k$ multiplexed interferometer. The conventions used here are the same as defined in Table I.

Pulse	Area	Time t_0	r_0	Direction	Detuning (ω_r)	Upper Path	Lower Path
1	$\pi/2$	$-\frac{L}{c}$	r_{in}	$\rightarrow$	1	$\|g,0\rangle \rightarrow \|e,\hbar k\rangle$	$\|g,0\rangle$
2	π	$-\tau$	r_{out}	$\leftarrow$	1	$\|e,\hbar k\rangle$	$\|g,0\rangle \rightarrow \|e,-\hbar k\rangle$
3	π	τ	r_{out}	$\leftarrow$	-3	$\|e,\hbar k\rangle \rightarrow \|g,2\hbar k\rangle$	$\|e,-\hbar k\rangle$
4	π	$\frac{L}{c}$	r_{in}	$\rightarrow$	-3	$\|g,2\hbar k\rangle$	$\|e,-\hbar k\rangle \rightarrow \|g,-2\hbar k\rangle$
5	π	$\frac{T}{9}-\frac{L}{c}-2\tau$	r_{out}	$\leftarrow$	5	$\|g,2\hbar k\rangle$	$\|g,-2\hbar k\rangle \rightarrow \|e,-3\hbar k\rangle$
6	π	$\frac{T}{9}-\tau$	r_{in}	$\rightarrow$	-7	$\|g,2\hbar k\rangle$	$\|e,-3\hbar k\rangle \rightarrow \|g,-4\hbar k\rangle$
7	π	$\frac{T}{9}+\tau$	r_{in}	$\rightarrow$	5	$\|g,2\hbar k\rangle \rightarrow \|e,3\hbar k\rangle$	$\|g,-4\hbar k\rangle$
8	π	$\frac{T}{9}+\frac{L}{c}+2\tau$	r_{out}	$\leftarrow$	-7	$\|e,3\hbar k\rangle \rightarrow \|g,4\hbar k\rangle$	$\|g,-4\hbar k\rangle$
9	π	$\frac{2T}{9}-\frac{L}{c}-2\tau$	r_{in}	$\rightarrow$	9	$\|g,4\hbar k\rangle \rightarrow \|e,5\hbar k\rangle$	$\|g,-4\hbar k\rangle$
10	π	$\frac{2T}{9}-\tau$	r_{out}	$\leftarrow$	-11	$\|e,5\hbar k\rangle \rightarrow \|g,6\hbar k\rangle$	$\|g,-4\hbar k\rangle$
11	π	$\frac{2T}{9}+\tau$	r_{out}	$\leftarrow$	9	$\|g,6\hbar k\rangle$	$\|g,-4\hbar k\rangle \rightarrow \|e,-5\hbar k\rangle$
12	π	$\frac{2T}{9}+\frac{L}{c}+2\tau$	r_{in}	$\rightarrow$	-11	$\|g,6\hbar k\rangle$	$\|e,-5\hbar k\rangle \rightarrow \|g,-6\hbar k\rangle$
13	π	$\frac{5T}{9}-\frac{L}{c}$	r_{out}	$\leftarrow$	-11	$\|g,6\hbar k\rangle \rightarrow \|e,5\hbar k\rangle$	$\|g,-6\hbar k\rangle$
14	π	$\frac{5T}{9}-\tau$	r_{in}	$\rightarrow$	-11	$\|e,5\hbar k\rangle$	$\|g,-6\hbar k\rangle \rightarrow \|e,-5\hbar k\rangle$
15	π	$\frac{5T}{9}+\tau$	r_{in}	$\rightarrow$	9	$\|e,5\hbar k\rangle \rightarrow \|g,4\hbar k\rangle$	$\|e,-5\hbar k\rangle$
16	π	$\frac{5T}{9}+\frac{L}{c}$	r_{out}	$\leftarrow$	9	$\|g,4\hbar k\rangle$	$\|e,-5\hbar k\rangle \rightarrow \|g,-4\hbar k\rangle$
17	π	$\frac{7T}{9}-\frac{L}{c}$	r_{out}	$\leftarrow$	-7	$\|g,4\hbar k\rangle \rightarrow \|e,3\hbar k\rangle$	$\|g,-4\hbar k\rangle$
18	π	$\frac{7T}{9}-\tau$	r_{in}	$\rightarrow$	-7	$\|e,3\hbar k\rangle$	$\|g,-4\hbar k\rangle \rightarrow \|e,-3\hbar k\rangle$
19	π	$\frac{7T}{9}+\tau$	r_{in}	$\rightarrow$	5	$\|e,3\hbar k\rangle \rightarrow \|g,2\hbar k\rangle$	$\|e,-3\hbar k\rangle$
20	π	$\frac{7T}{9}+\frac{L}{c}$	r_{out}	$\leftarrow$	5	$\|g,2\hbar k\rangle$	$\|e,-3\hbar k\rangle \rightarrow \|g,-2\hbar k\rangle$
21	π	$T-\frac{2L}{c}-3\tau$	r_{in}	$\rightarrow$	-3	$\|g,2\hbar k\rangle$	$\|g,-2\hbar k\rangle \rightarrow \|e,-\hbar k\rangle$
22	π	$T-\frac{L}{c}-2\tau$	r_{out}	$\leftarrow$	1	$\|g,2\hbar k\rangle$	$\|e,-\hbar k\rangle \rightarrow \|g,0\rangle$
23	π	$T-\frac{L}{c}-\tau$	r_{out}	$\leftarrow$	-3	$\|g,2\hbar k\rangle \rightarrow \|e,\hbar k\rangle$	$\|g,0\rangle$
24	π	T	r_{in}	$\rightarrow$	1	$\|e,\hbar k\rangle \rightarrow \|g,0\rangle$	$\|g,0\rangle \rightarrow \|e,\hbar k\rangle$
25	π	$T+\frac{L}{c}+\tau$	r_{out}	$\leftarrow$	-3	$\|g,0\rangle$	$\|e,\hbar k\rangle \rightarrow \|g,2\hbar k\rangle$
26	π	$T+\frac{L}{c}+2\tau$	r_{out}	$\leftarrow$	1	$\|g,0\rangle \rightarrow \|e,-\hbar k\rangle$	$\|g,2\hbar k\rangle$
27	π	$T+\frac{2L}{c}+3\tau$	r_{in}	$\rightarrow$	-3	$\|e,-\hbar k\rangle \rightarrow \|g,-2\hbar k\rangle$	$\|g,2\hbar k\rangle$
28	π	$\frac{10T}{9}-\frac{L}{c}-2\tau$	r_{in}	$\rightarrow$	5	$\|g,-2\hbar k\rangle$	$\|g,2\hbar k\rangle \rightarrow \|e,3\hbar k\rangle$
29	π	$\frac{10T}{9}-\tau$	r_{out}	$\leftarrow$	-7	$\|g,-2\hbar k\rangle$	$\|e,3\hbar k\rangle \rightarrow \|g,4\hbar k\rangle$
30	π	$\frac{10T}{9}+\tau$	r_{out}	$\leftarrow$	5	$\|g,-2\hbar k\rangle \rightarrow \|e,-3\hbar k\rangle$	$\|g,4\hbar k\rangle$
31	π	$\frac{10T}{9}+\frac{L}{c}+2\tau$	r_{in}	$\rightarrow$	-7	$\|e,-3\hbar k\rangle \rightarrow \|g,-4\hbar k\rangle$	$\|g,4\hbar k\rangle$
32	π	$\frac{11T}{9}-\frac{L}{c}-2\tau$	r_{out}	$\leftarrow$	9	$\|g,-4\hbar k\rangle \rightarrow \|e,-5\hbar k\rangle$	$\|g,4\hbar k\rangle$
33	π	$\frac{11T}{9}-\tau$	r_{in}	$\rightarrow$	-11	$\|e,-5\hbar k\rangle \rightarrow \|g,-6\hbar k\rangle$	$\|g,4\hbar k\rangle$
34	π	$\frac{11T}{9}+\tau$	r_{in}	$\rightarrow$	9	$\|g,-6\hbar k\rangle$	$\|g,4\hbar k\rangle \rightarrow \|e,5\hbar k\rangle$
35	π	$\frac{11T}{9}+\frac{L}{c}+2\tau$	r_{out}	$\leftarrow$	-11	$\|g,-6\hbar k\rangle$	$\|e,5\hbar k\rangle \rightarrow \|g,6\hbar k\rangle$
36	π	$\frac{14T}{9}-\frac{L}{c}$	r_{in}	$\rightarrow$	-11	$\|g,-6\hbar k\rangle \rightarrow \|e,-5\hbar k\rangle$	$\|g,6\hbar k\rangle$
37	π	$\frac{14T}{9}-\tau$	r_{out}	$\leftarrow$	-11	$\|e,-5\hbar k\rangle$	$\|g,6\hbar k\rangle \rightarrow \|e,5\hbar k\rangle$
38	π	$\frac{14T}{9}+\tau$	r_{out}	$\leftarrow$	9	$\|e,-5\hbar k\rangle \rightarrow \|g,-4\hbar k\rangle$	$\|e,5\hbar k\rangle$
39	π	$\frac{14T}{9}+\frac{L}{c}$	r_{in}	$\rightarrow$	9	$\|g,-4\hbar k\rangle$	$\|e,5\hbar k\rangle \rightarrow \|g,4\hbar k\rangle$
40	π	$\frac{16T}{9}-\frac{L}{c}$	r_{in}	$\rightarrow$	-7	$\|g,-4\hbar k\rangle \rightarrow \|e,-3\hbar k\rangle$	$\|g,4\hbar k\rangle$
41	π	$\frac{16T}{9}-\tau$	r_{out}	$\leftarrow$	-7	$\|e,-3\hbar k\rangle$	$\|g,4\hbar k\rangle \rightarrow \|e,3\hbar k\rangle$
42	π	$\frac{16T}{9}+\tau$	r_{out}	$\leftarrow$	5	$\|e,-3\hbar k\rangle \rightarrow \|g,-2\hbar k\rangle$	$\|e,3\hbar k\rangle$
43	π	$\frac{16T}{9}+\frac{L}{c}$	r_{in}	$\rightarrow$	5	$\|g,-2\hbar k\rangle$	$\|e,3\hbar k\rangle \rightarrow \|g,2\hbar k\rangle$
44	π	$2T-\frac{L}{c}-2\tau$	r_{in}	$\rightarrow$	-3	$\|g,-2\hbar k\rangle \rightarrow \|e,-\hbar k\rangle$	$\|g,2\hbar k\rangle$
45	π	$2T-\tau$	r_{out}	$\leftarrow$	1	$\|e,-\hbar k\rangle \rightarrow \|g,0\rangle$	$\|g,2\hbar k\rangle$
46	π	$2T+\tau$	r_{out}	$\leftarrow$	-3	$\|g,0\rangle$	$\|g,2\hbar k\rangle \rightarrow \|e,\hbar k\rangle$
47	$\pi/2$	$2T+\frac{L}{c}+2\tau$	r_{in}	$\rightarrow$	1	$\|g,0\rangle \rightarrow \|e,\hbar k\rangle$	$\|e,\hbar k\rangle \rightarrow \|g,0\rangle$

Here $\text{Cin}(x) \equiv \int_0^x \frac{1-\cos t}{t} dt$ is an alternate form of the cosine integral [13]. The 53 coefficients Λ_n that appear in the sums in Eq. (11) are integers and are shown in Fig. 2. Equation (11) assumes that the interferometer time T is set to the minimum value allowed by the propagation time of the pulses back and forth across the baseline: $T = 27(\frac{L}{c} + 2\tau)$. The $12\hbar k$ sensitivity curve shown in Fig. 3 represents an average of several T just like the $2\hbar k$ case, but here for simplicity we only give the result using the minimum T. For similar reasons, we have also taken $\tau \ll \frac{L}{c}$ in writing Eq. (11).

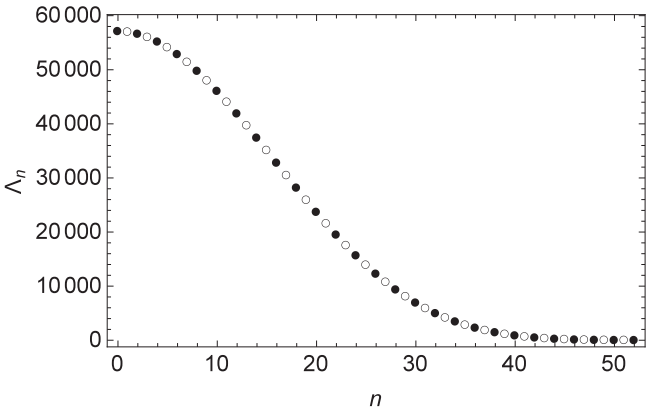

FIG. 2. Integer coefficients Λ_n that appear in Eq. (11). Even and odd coefficients are shown as solid and open circles, respectively.

IV. SENSITIVITY

Figure 3 shows the strain sensitivity curves for two long-baseline designs using Sr atoms. The more conservative design (green) uses an $L = 2 \times 10^9$ m baseline and the photon shot-noise limited laser link assumes 1 W laser power, a $d = 30$ cm diameter telescope, and a repetition rate $f_R = 0.2$ Hz [14]. The long baseline allows for high sensitivity even though the design assumes conservative $2\hbar k$ atom optics and atom shot noise of $\overline{\delta\phi}_a = 10^{-3}$ rad/$\sqrt{\text{Hz}}$. A long interrogation time of $T = 160$ s is used to support low-frequency sensitivity, but despite this long drift time the maximum wave-packet separation is bounded to <2 m. The atom source design assumes ensembles of 7×10^6 atoms with a 20-pK longitudinal temperature, allowing for a $\Omega/2\pi = 60$ Hz Rabi frequency. Such design criteria are readily met using existing technology [15].

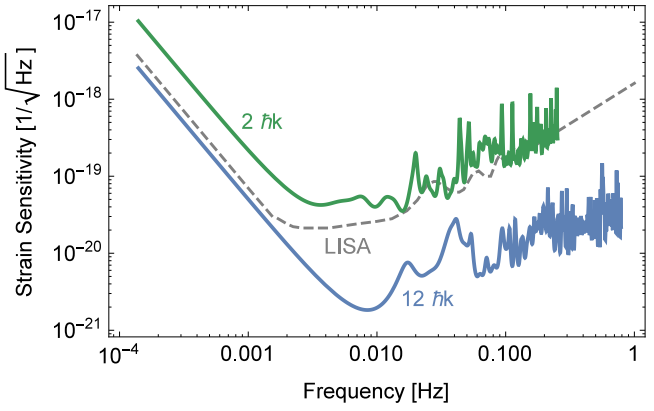

FIG. 3. Strain sensitivity for a $2\hbar k$ Sr interferometer with baseline $L = 2 \times 10^9$ m (green) as well as a $12\hbar k$ interferometer with baseline $L = 6 \times 10^8$ m (blue). The strain responses have been averaged over gravitational-wave propagation direction and polarization. The $2\hbar k$ curve represents an average of three alternating interferometer interrogation times: $T = 160$ s, 100 s, 40 s. The $12\hbar k$ curve is an average of $T = 75$ s, 69 s, 59 s, 53 s, limited at the low end by the light travel time. The interrogation time average regularizes the detector response by suppressing well-known notches in single interferometer transfer functions [4]. The LISA strain curve is shown for reference [3].

LMT techniques allow for enhanced sensitivity, as shown by the second strain sensitivity curve (blue) in Fig. 3. This design is based on a $12\hbar k$ interferometer sequence with an $L = 6 \times 10^8$ m baseline and improved phase noise $\overline{\delta\phi}_a = 10^{-4}$ rad/$\sqrt{\text{Hz}}$. Photon shot-noise requirements are met using 1 W laser power and a $d = 50$ cm diameter telescope, giving Rabi frequency $\Omega/2\pi = 40$ Hz. The design has a sampling rate of $f_R = 1$ Hz. The increased phase sensitivity of this design allows for improved low-frequency response even using a smaller interrogation time. Using $T = 75$ s, the maximum wave-packet separation is <4 m.

V. NOISE ANALYSIS

A. Timing jitter

Another source of noise is timing delay and jitter in the pulses emitted by the phase-locked local oscillator laser. Referring to Fig. 1, consider a pulse emitted from M1 at time t that arrives at the satellite 2 beam splitter at time t_a. If the pulse emitted from LO2 is offset by some time t_d with respect to the arrival of the reference pulse, the laser phase $\phi_{LO}(t_a + t_d)$ imprinted on interferometer 2 will be different from the phase $\phi_M(t)$ written onto interferometer 1 by the amount $\phi_{LO}(t_a + t_d) - \phi_M(t) = \overline{\omega} t_d + \delta\phi$, where $\overline{\omega} \equiv \frac{1}{t_d}\int_{t_a}^{t_a+t_d} \omega(t')dt'$ is the average frequency of laser LO2 during the timing delay and $\delta\phi \equiv \phi_{LO}(t_a) - \phi_M(t)$ quantifies any imperfection in the phase lock between R1 and LO2. In addition, the time skewed transition in interferometer 2 implies that interferometer 1 spends a different time in the excited state by comparison, leading to an extra differential phase $\omega_A t_d$ for excited state energy $\hbar\omega_A$ [16]. The total differential phase is then $\Delta\phi_{\text{delay}} = (\overline{\omega} - \omega_A)t_d + \delta\phi$. Noise in $\delta\phi$ from an imperfect phase reference was discussed above [Eq. (1)]. Additional noise due to the delayed pulse can arise from either timing jitter $\overline{\delta t}_d$ or frequency noise $\overline{\delta\omega}$, giving a noise PSD of $\overline{\delta\phi}^2_{\text{delay}} = (N\, t_d\, \overline{\delta\omega})^2 + (N\, \Delta\, \overline{\delta t}_d)^2$, where $\Delta = \overline{\omega} - \omega_A$ is the pulse detuning and N is the LMT phase enhancement factor. Keeping each term below $\overline{\delta\phi}_a$ requires noise amplitude spectral densities of

$$\overline{\delta\omega} = 2\pi \times 80 \frac{\text{Hz}}{\sqrt{\text{Hz}}} \left(\frac{2}{N}\right)\left(\frac{1\ \mu\text{s}}{t_d}\right)\left(\frac{\overline{\delta\phi}_a}{10^{-3}\ \text{rad}/\sqrt{\text{Hz}}}\right), \quad (12)$$

$$\overline{\delta t}_d = 1.3 \frac{\mu\text{s}}{\sqrt{\text{Hz}}} \left(\frac{2}{N}\right)\left(\frac{60\ \text{Hz}}{\Delta/2\pi}\right)\left(\frac{\overline{\delta\phi}_a}{10^{-3}\ \text{rad}/\sqrt{\text{Hz}}}\right) \quad (13)$$

at frequencies in the GW detection band. In particular, this shows that the long-time frequency stability requirements of the LO laser can be reduced by ensuring that the pulses from the LO are well synchronized with the incoming reference pulses, keeping t_d small. In practice, $t_d \sim 10$ ns with rms noise $\delta t_d \sim 1$ ns appears straightforward, suggesting that LO pulse timing constraints are manageable.

B. Pointing jitter

Satellite and laser beam pointing jitter can also introduce noise. Consider a beam propagating approximately along the z axis in Fig. 1 from satellite 1 towards satellite 2 that is tilted by a small angle θ_y about the y axis. Near satellite 1, the

phase of the Gaussian beam varies with position as $\Phi_1(x,z) \approx kz + k\theta_y x$, where the center of rotation of the beam is taken to be $x = 0$, $z = 0$. By comparison, the phase near satellite 2 is $\Phi_2(x,z) \approx k(z+L) + k\theta_y (z_R/L)^2 x$ for baseline length L much longer than the Rayleigh range z_R. Here a long baseline is advantageous since when $z_R \ll L$ the beam arriving at satellite 2 is approximately a spherical wave, so the dependence of the phase on angle is greatly suppressed. In this limit, the pointing jitter constraint is set by the Φ_1 coupling and has noise amplitude $\overline{\delta\phi}_\theta = 4kN\Delta x\,\overline{\delta\theta}$, where $\overline{\delta\theta}^2$ is the angle noise PSD and Δx is the transverse position offset of the atom relative to the baseline [17,18]. The pointing requirement is then

$$\overline{\delta\theta} = 10\frac{\text{nrad}}{\sqrt{\text{Hz}}}\left(\frac{2}{N}\right)\left(\frac{1\text{ mm}}{\Delta x}\right)\left(\frac{\overline{\delta\phi}_a}{10^{-3}\text{ rad}/\sqrt{\text{Hz}}}\right). \quad (14)$$

To avoid introducing additional pointing noise, the LO laser beam incident on the atoms must point in the same direction as the incoming reference laser pulse. This can be facilitated by monitoring the relative angle between the two beams at the beamsplitter. In addition to measuring the beat note for the phase reference, a position sensitive detector such as as quadrant photodiode can be used to record the spatial interference pattern between the reference and LO beams. Feedback applied to a tip-tilt mirror (show as TTM in Fig. 1 before the BS) can then be used to control the angle of the LO laser. Similarly, the angle of the master laser itself can be controlled by comparing it to the LO laser direction and using another tip-tilt mirror. The interference signal between the LO and the master can be generated using a Michelson interferometer geometry, inserting an additional beam splitter at any point along the path where the two beams are counterpropagating. In this configuration, the pointing stability of all the beams is tied to the stability of the incoming (nearly) spherical wave fronts of the reference beam.

The performance of the angle control loop is ultimately limited by the shot noise of the received reference wave front. To estimate this, note that the power difference ΔP between the two sides of a quadrant detector due to the spatial interference pattern caused by a small angle $\Delta\theta$ between the LO and the reference beam is $\Delta P \approx 4\sqrt{2\pi}\sqrt{P_{LO}P_r}\Delta\theta\, w_t/\lambda$ for a telescope diameter $d = 2w_t$ and received powers P_{LO} and P_r from the two beams [19]. The noise in ΔP is dominated by the strong LO beam, giving a noise PSD of $\overline{\delta(\Delta P)}^2 \approx \overline{\delta P}^2_{LO} = h\nu P_{LO}$ assuming shot noise for the LO optical power noise. The shot-noise limit for a measurement of $\Delta\theta$ is then given by amplitude spectral density

$$\overline{\delta(\Delta\theta)} = \frac{\sqrt{S_{\text{sh}}}}{4\sqrt{2\pi}}\frac{\lambda}{w_t} \approx 1\frac{\text{nrad}}{\sqrt{\text{Hz}}}\left(\frac{10\text{cm}}{w_t}\right)\left(\frac{\overline{\delta\phi}_a}{10^{-3}\text{ rad}/\sqrt{\text{Hz}}}\right), \quad (15)$$

where $S_{\text{sh}} = h\nu/P_r$ is the phase noise PSD of the reference beam and we assume a design with $S_{\text{sh}} = \overline{\delta\phi}_a^2$ as before. Comparing this with the requirement in Eq. (14) suggests that the angle can be sufficiently well measured to control the LO pointing direction. This also suggests that overall satellite bus pointing requirements are modest ($\sim 10^{-6}$ rad/$\sqrt{\text{Hz}}$, limited by the dynamic range of the pointing servos), and substantially reduced from previous proposals.

C. Wave-front aberrations

Past atom-based designs have required large momentum transfer to reach design sensitivity. The designs proposed here operate at lower momentum transfer and thus place much less stringent constraints on laser phase front stability. For example, here we require a phase stability of $\lambda/30$ for the telescope. Following Refs. [4,18,20,21], laser wave-front aberrations $\delta\lambda/\lambda$ couple to satellite transverse position noise $\overline{\delta x}$, resulting in phase noise amplitude $\overline{\delta\phi}_\lambda = 16\pi^2 N(\delta\lambda/\lambda)\overline{\delta x}/\Lambda$, where Λ is the aberration wavelength [17]. The estimated wave-front requirement for the interferometer beam is then [22]

$$\delta\lambda = \frac{\lambda}{30}\left(\frac{2}{N}\right)\left(\frac{\Lambda}{1\text{cm}}\right)\left(\frac{\overline{\delta\phi}_a}{10^{-3}\text{ rad}/\sqrt{\text{Hz}}}\right)\left(\frac{1\mu\text{m}/\sqrt{\text{Hz}}}{\overline{\delta x}}\right). \quad (16)$$

For example, a $\overline{\delta x} = 1\mu\text{m}/\sqrt{\text{Hz}}$ satellite transverse position jitter implies a telescope mirror quality of $\lambda/30$. This suggests modest satellite bus jitter and telescope mirror polish requirements.

D. Local forces

Instrument constraints imposed by backgrounds that have their origin in spurious forces or phase shifts (due to, for example, magnetic-field gradients, blackbody shifts, ac Stark shifts, or gravitational gradients) are significantly eased due to the longer baseline. Since previous shorter baseline designs could meet these requirements [23], in the longer baseline designs proposed here these backgrounds can be brought to levels where they do not impact instrument performance. Tight (~ 0.1 mK/Hz$^{1/2}$) thermal control over the temperature of the beamsplitter is required to suppress thermally induced path length fluctuations of the glass [24].

E. Gravity gradient noise

Acceleration noise arising from the gravitational gradient of the spacecraft [18,25,26] is an important consideration in the current design, since unlike previous proposals here the atoms are kept inside the spacecraft. However, with appropriate design of the spacecraft mass distribution, the gravity gradient can be reduced to $<10E$ in the interferometry region, allowing for sufficient noise suppression with only modest spacecraft jitter requirements (see Fig. 4).

The gravitational interaction between the atoms and the spacecraft can cause spurious acceleration noise due to uncontrolled motion of the satellite. To model this, we consider an atom at position $\mathbf{r}$ and take the nominal gravitational potential from the spacecraft at this point to be $\widetilde{\phi}(\mathbf{r})$. If the source of $\widetilde{\phi}(\mathbf{r})$ (the spacecraft) is displaced by some amount $+\delta\mathbf{R}(t)$, then the potential at position $\mathbf{r}$ is translated such that the atom will see a potential

$$\phi(\mathbf{r},t) = \widetilde{\phi}(\mathbf{r} - \delta\mathbf{R}(t)). \quad (17)$$

We assume the displacement noise is small so that we can expand to first order in $\delta\mathbf{R}(t)$,

$$\phi(\mathbf{r},t) \approx \widetilde{\phi}(\mathbf{r}) + \widetilde{\mathbf{g}}(\mathbf{r})\cdot\delta\mathbf{R}(t), \quad (18)$$

where $\widetilde{\mathbf{g}}(\mathbf{r}) \equiv -\nabla\widetilde{\phi}(\mathbf{r})$ is the nominal gravitational field of the spacecraft. The ith component of the gravitational field at the

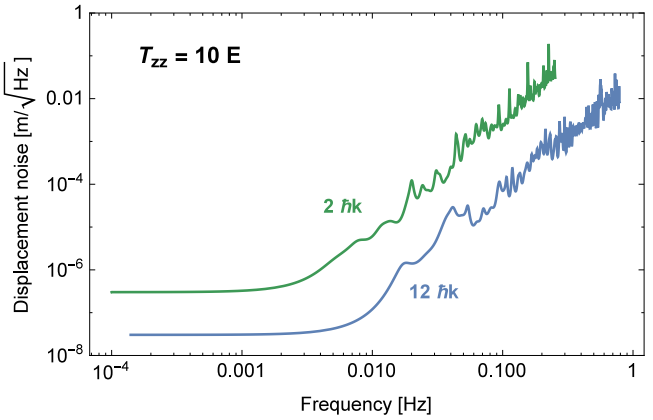

FIG. 4. Spacecraft jitter requirement due to gravity gradient noise. The two curves are for the $2\hbar k$ (green) and $12\hbar k$ (blue) interferometer modes. The constraints assume a residual gravity gradient after compensation of $T_{zz} = 10E$.

point of the atom ($\mathbf{g} = -\nabla\phi$) is then

$$g_i(\mathbf{r},t) = \widetilde{g}_i(\mathbf{r}) + T_{ij}(\mathbf{r})\,\delta R_j(t), \tag{19}$$

where $T_{ij}(\mathbf{r}) = \partial_i\partial_j\phi(\mathbf{r})$ is the gravity gradient tensor at the position of the atom.

A local acceleration $\mathbf{g}(\mathbf{r},t)$ applied to only one of the atom interferometers will not be common mode suppressed in the gradiometer signal and will contribute to the background noise of the detector. The phase response to a local acceleration can be calculated in a straightforward manner by first determining the modified trajectory of the atom. We assume a sinusoidal position jitter $\delta R_z(t) = \delta R\cos(\omega t - \phi_0)$ and consider the response along the sensitive axis of the detector, which here we take to be the z axis. The resulting acceleration causes the atom path to deviate from the fixed coordinate position assumed in Sec. III, effectively changing the baseline distance between the two interferometers. This affects the arrival times of the photon geodesics at the position of the atom, which in turn changes the amount of time the atom spends in the excited state.

For the $2\hbar k$ interferometer, the rms gravity gradient phase shift amplitude due to $\delta R_z(t)$ jitter at frequency ω is

$$\Delta\Phi_{\rm gg} = 8\frac{\omega_a}{c}\frac{T_{zz}\,\delta R}{\omega^2}\sin^2\left(\frac{\omega T}{2}\right), \tag{20}$$

where for simplicity we assume $\tau \ll T$ and $L/c \ll T$. For comparison, the GW signal given by Eq. (9) in the same limit is

$$\Delta\Phi^{\rm rms}_{2\hbar k} \approx \frac{8}{\sqrt{15}}\frac{\omega_a}{c}h_{\rm rms}L\,\sin^2\left(\frac{\omega T}{2}\right), \tag{21}$$

where we also have taken $\omega L/c \ll 1$. The constraints on δR follow from setting $\Delta\Phi_{\rm gg} = \Delta\Phi^{\rm rms}_{2\hbar k}$ for a given target $h_{\rm rms}(\omega)$. To achieve the sensitivity curves in Fig. 3 of the main text, the constraints for the $2\hbar k$ and $12\hbar k$ interferometer modes are shown in Fig. 4. These constraints assume a target gravity gradient in the interferometer region of $T_{zz} = 10E$.

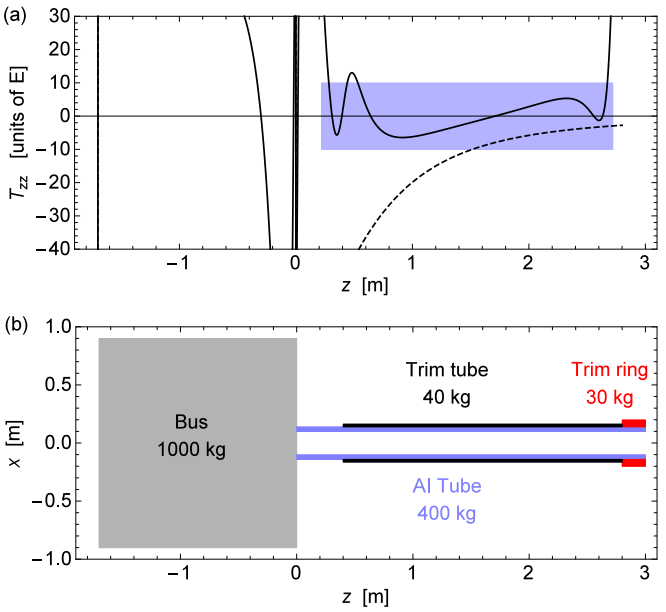

FIG. 5. Gravity gradient compensation model. (a) Gravity gradients T_{zz} due to the spacecraft bus, interferometer vacuum tube, and trim masses (solid curve). The dashed curve shows the gravity gradient from the spacecraft bus alone without any compensation masses. The blue shaded area is the 2.5-m-long atom-interferometer region where the compensated rms gravity gradient is less than $10E$. (b) Example spacecraft design leading to the gravity gradient shown in (a). The sizes and masses of the spacecraft bus (gray), atom-interferometry tube (blue), and two trim masses (black and red) are shown. All elements are assumed to be cylindrically symmetric about the z axis, which is also the sensitive axis of the atom interferometer. The atom-interferometry (AI) tube and both trim masses are taken to have the density of titanium. For clarity, the radial dimensions (here x) of the trim masses are shown exaggerated.

The spacecraft can be designed to reduce the gravity gradient to this level.

The gravity gradient that the atoms experience is dependent on the mass distribution of the spacecraft. Assuming a design in which the atom-interferometer science instrument is attached adjacent to a conventional spacecraft bus, there can be a significant gravity gradient arising from the bus. Trim masses can be use to compensate for this gravity gradient to reduce T_{zz} to required levels. Figure 5 shows one particular arrangement of trim masses and the resulting gravity gradient. This model uses a spacecraft bus with realistic size and mass and assumes that the interferometer vacuum tube and trim masses are made out of titanium (density 4.5 g/cm^3). All elements in the model are assumed to be cylindrically symmetric about the detector baseline direction (here the z axis). This shows that with appropriate choice of trim mass geometry it is possible to reduce the gravity gradient in the interferometer region to $T_{zz} \sim 10E$.

VI. DISCUSSION

Several variations of the basic laser link concept are possible. For example, by employing a second laser link on each satellite, a dedicated reference laser can be used

to generate the reference beams instead of relying on the transmitted master laser light as shown in Fig. 1. In this modified setup, the heterodyne signal between the master laser and the new reference laser is formed on the existing beamsplitter (BS) such that the reflected reference laser beam is directed towards the opposite satellite.

Generalizing further, if the reference beam is a separate laser then in principle its wavelength can be different from that of the atomic transition. An optical frequency comb would then be used to implement the heterodyne lock, spanning the frequency difference between the reference laser and the lasers responsible for interrogating the atoms. Changing the reference wavelength could lead to lower optical shot noise [$\sim\lambda^{5/4}$ in Eq. (1)] or could exploit existing laser technology at particular wavelengths.

The degree to which polarization and sky position information of a gravitational-wave source is available with a single-arm detector depends on the lifetime of the source and the orbit period of the detector, and requires further analysis. This information is also available using constellations of multiple pairs of single-baseline instruments.

ACKNOWLEDGMENTS

The authors would like to acknowledge J. Baker, J. Livas, I. Thorpe, and S. Vitale for valuable discussions. This work was supported in part by the NASA NIAC program and the W. M. Keck Foundation.

[1] The properties of the atomic proof masses are regular (all atoms are identical) and knowable (well defined magnetic susceptibility). They are immune from charging events.

[2] P. W. Graham, J. M. Hogan, M. A. Kasevich, and S. Rajendran, Phys. Rev. Lett. **110**, 171102 (2013).

[3] LISA Study Team, LISA Pre-Phase A Report, 1998.

[4] S. Dimopoulos, P. W. Graham, J. M. Hogan, M. A. Kasevich, and S. Rajendran, Phys. Rev. D **78**, 122002 (2008).

[5] S.-w. Chiow, T. Kovachy, H.-C. Chien, and M. A. Kasevich, Phys. Rev. Lett. **107**, 130403 (2011).

[6] S.-w. Chiow, J. Williams, and N. Yu, Phys. Rev. A **92**, 063613 (2015).

[7] All lasers must have sufficiently narrow linewidth to drive the atomic transitions. They also must be appropriately frequency offset to accommodate Doppler shifts due to the relative velocity of the spacecraft.

[8] The weighting function $w(t)$ can be shown to be normalized such that $\frac{1}{\tau}\int_{t_0}^{t_0+\tau} w(t)dt = 1$ for a π pulse.

[9] G. J. Dick, J. D. Prestage, C. A. Greenhall, and L. Maleki, Local Oscillator Induced Degradation of Medium-Term Stability in Passive Atomic Frequency Standards, Tech. Rep. (DTIC Document, 1990).

[10] P. Cheinet, B. Canuel, F. Pereira Dos Santos, A. Gauguet, F. Yver-Leduc, and A. Landragin, IEEE Trans. Instrum. Meas. **57**, 1141 (2008).

[11] To accommodate Doppler shifts due to the initial relative velocity of the satellites, the LO can be offset locked to the reference, or a tunable sideband on the LO laser can be used to interrogate the atoms.

[12] M. Rakhmanov, Classical Quantum Gravity **26**, 155010 (2009).

[13] This less common alternate form is related to the usual cosine integral $\mathrm{Ci}(x)$ by $\mathrm{Cin}(x) = -\mathrm{Ci}(x) + \ln x + \gamma$, where γ is the Euler-Mascheroni constant.

[14] Such a repetition rate can be realized by running concurrent interferometers, implemented using different initial velocities so that each interferometer is addressable with a unique Doppler shift. Strategies for efficient allocation of Doppler bandwidth for LMT interferometers are discussed in [27].

[15] T. Kovachy, J. M. Hogan, A. Sugarbaker, S. M. Dickerson, C. A. Donnelly, C. Overstreet, and M. A. Kasevich, Phys. Rev. Lett. **114**, 143004 (2015).

[16] The description here is of a transition from the ground to excited state. For transitions from excited to ground, the signs of all the phase shifts are flipped.

[17] Assumes a conventional $\pi/2 - \pi - \pi/2$ $N\hbar k$ LMT sequence and a perturbation frequency $\omega = \pi/T$ equal to the peak GW response frequency.

[18] J. M. Hogan, D. M. S. Johnson, S. Dickerson, T. Kovachy, A. Sugarbaker, S.-w. Chiow, P. W. Graham, M. A. Kasevich, B. Saif, S. Rajendran, P. Bouyer, B. D. Seery, L. Feinberg, and R. Keski-Kuha, Gen. Relativ. Gravity **43**, 1953 (2011).

[19] See, for example, [28].

[20] P. L. Bender, Phys. Rev. D **84**, 028101 (2011).

[21] S. Dimopoulos, P. W. Graham, J. M. Hogan, M. A. Kasevich, and S. Rajendran, Phys. Rev. D **84**, 028102 (2011).

[22] See Eq. (6) of Ref. [18]. Here we neglect averaging over the cloud. Averaging would further relax requirements at short wavelengths.

[23] See, for example, the analysis in Refs. [2,18].

[24] These arise from thermal expansion of the glass and temperature induced changes in the index of refraction of the glass.

[25] R. T. Stebbins, P. L. Bender, J. Hanson, C. D. Hoyle, B. L. Schumaker, and S. Vitale, Classical Quantum Gravity **21**, S653 (2004).

[26] S. M. Merkowitz, W. B. Haile, S. Conkey, W. Kelly, and H. Peabody, Classical Quantum Gravity **22**, S395 (2005).

[27] J. M. Hogan (unpublished).

[28] J. M. Hogan, J. Hammer, S.-W. Chiow, S. Dickerson, D. M. S. Johnson, T. Kovachy, A. Sugarbaker, and M. A. Kasevich, Opt. Lett. **36**, 1698 (2011).